Ceramics International 43 (2017) 7172–7176

Contents lists available at ScienceDirect

Ceramics International

journal homepage: www.elsevier.com/locate/ceramint

Synthesis and characterization of high-density B_2O_3-added forsterite ceramics

Suminar Pratapa[a,*], Wahyu Dwi Handoko[a], Upik Nurbaiti[a,b], Mashuri[a]

[a] Department of Physics, Faculty of Mathematics and Sciences, Institute of Technology Sepuluh Nopember (ITS), Jl. Arief Rahman Hakim, Surabaya 60111, Indonesia

[b] Department of Physics, Faculty of Mathematics and Natural Sciences, Semarang State University, Jl. Raya Sekaran Gunung Pati, Semarang 50221, Indonesia

ARTICLE INFO

Keywords:
Forsterite ceramics
B_2O_3 addition
Silica sand
Ultra-density ceramics
Vickers hardness
Dielectric constant

ABSTRACT

Boria (B_2O_3)-added forsterite (Mg_2SiO_4) ceramics were synthesized and their properties were characterized. The addition of B_2O_3 was aimed to produce high density forsterite ceramics at a low sintering temperature. The raw materials were purified silica sand and commercial magnesia powders. Fosterite powder was produced from a solid reaction between the raw powders at 1100 °C prior to addition of B_2O_3, uniaxial pressing and sintering at 1200 °C. The amount of added B_2O_3 varied between 0%, 4%, and 8% by weight. Elemental analysis was performed by X-ray fluorescence (XRF) spectroscopy on the purified silica powder, whereas phase analyses were obtained from X-ray diffraction (XRD) data. Characterization of the ceramics included diameter shrinkage, density-porosity, thermal expansion, Vickers hardness, and dielectric constant. The results showed that the silica powder contained 98.7 at% Si with minor impurities, including 0.5 at% Ti, but the only identified crystalline phase was quartz. Further phase analysis of the ceramics showed that the addition of B_2O_3 reduced the amount of formed forsterite and increased the amount of cristobalite, proto- and clino-enstatite ($MgSiO_3$) as well as suanite ($Mg_2B_2O_5$). The highest forsterite content was found in B_2O_3-free ceramics, approximately 88.1 wt%. Moreover, the addition of B_2O_3 also reduced the diameter of the sample by more than 21%, resulting in a very dense ceramic with an apparent porosity of only 0.3%. The Vickers hardness significantly increased from 0.3 GPa for the B_2O_3-free ceramic to 10.9 GPa for the 4% B_2O_3 sample. The dielectric constant of the B_2O_3-added forsterite ceramics was improved by approximately 2–6 times that of the B_2O_3-free ceramic, which was primarily attributed to the loss of porosity in the samples.

1. Introduction

Forsterite is a member of the Mg-Si-O ceramic systems with a chemical formula of Mg_2SiO_4. It is naturally discovered as an olivine mineral, but synthetic forms are now easily prepared. The latter exhibit physical properties that meet several criteria of functional and technological materials. The effectiveness of forsterite as a candidate for dental tissue [1] or millimeter-wave communication [2] engineering has been extensively studied. The wide range of applications is due to its specific properties, including a high fracture toughness value of up to 4.5–4.9 MPa $m^{1/2}$, a microhardness of approximately 7 GPa [3,4], a bending strength of approximately 200 MPa [5], and a *Q.f* value of up to 270,000 GHz as well as a relatively low dielectric constant of approximately 6.8 [2,4].

Synthetic forsterite has been fabricated in micrometric and nanometric powder forms [6,7] as well as in the form of ceramics [3,8,9]. Most studies used commercial raw materials, such as periclase (MgO), magnesium carbonate ($MgCO_3$), talc, magnesium nitrate hexahydrate, colloidal silica (SiO_2), silica powder or gel, and silicone resin [10–14]. Several syntheses of forsterite powder used natural or low-grade materials, such as rice husk ash [15], fumed silica [16] or silica sand [17] as the silica source. A small amount of forsterite was also found in a porcelain ceramic when natural talc was used [18]. To produce forsterite ceramics, forsterite powders are subjected to sintering, which, may require a temperature of more than 1400 °C [19]. From other studies, one possible way to produce ceramics at lower temperatures is through a glass-ceramic process. For example, the use of 1 wt% B_2O_3 as a sintering agent can reduce 8% of the porosity of a $Li_2ZnTi_3O_8$ ceramic at a sintering temperature of 875 °C [20].

In general, high-density ceramics are required for most applications. Tan dkk. [3] reported that processing periclase and talc powders in a solid-state reaction with a sintering temperature of 1200 °C

* Corresponding author.
E-mail address: suminar_pratapa@physics.its.ac.id (S. Pratapa).

http://dx.doi.org/10.1016/j.ceramint.2017.03.002
Received 1 February 2017; Received in revised form 21 February 2017; Accepted 1 March 2017
Available online 02 March 2017
0272-8842/ © 2017 Elsevier Ltd and Techna Group S.r.l. All rights reserved.

produced a forsterite ceramic with relatively low density, i.e., approximately 70%. Meanwhile, a combination of B_2O_3 and nepheline ($NaAlSiO_4$) significantly reduced the porosity of forsterite ceramics [15] that were sintered at 1000 °C. However, the relative density of the forsterite ceramics in this study was not reported. Nevertheless, the use of B_2O_3 has potential for producing high-density forsterite ceramics at a lower sintering temperature which hence revives the ceramic processing energy.

In this paper, we report the synthesis of very high-density forsterite ceramics using periclase powder and purified silica sand as the silica source with the addition of 4 wt% and 8 wt% B_2O_3. The B_2O_3-added ceramics exhibited ultra-low porosity, which is responsible for their unique physical characteristics. We describe here the phase composition, density and porosity, Vickers hardness, thermal expansion coefficient and dielectric properties of the ceramics.

2. Methods

The source of silica was purified natural silica sand that was taken from Tanah Laut, South Kalimantan. Purification included screening and washing, milling, magnetic separation, and immersion in 2 M hydrochloric acid as well as drying at room temperature to obtain a white silica powder. The other raw material was MgO powder (Merck), which contained some fraction of magnesium hydroxide ($Mg(OH)_2$). The powder was heated at 400 °C for 30 min to remove residual water. The purified silica powder and the treated MgO powder were mixed at a molar ratio of 1:2 and calcined at 1100 °C for 3 h to produce a powder with forsterite as the dominating phase. The powder was ground to a finer forsterite powder and mixed with B_2O_3 powder at 4% and 8% by weight as a sintering agent and with polyvinyl alcohol powder at 3% by weight as a binder prior to sintering at 1200 °C for 4 h. A specimen with no added B_2O_3 was also prepared as a control sample.

X-ray fluorescence (XRF) spectroscopy was used to determine the purity of the silica samples. Phase analyses were applied to the laboratory X-ray diffraction (XRD) data, which were collected using an Empyrean PANalytical XRD. The XRD used a Cu target and was operated at 40 kV and 30 mA with a 2θ-range between 10 and 65°2θ and a 0.017°2θ step-size. The phase composition analysis of the XRD data was conducted using *Rietica* software [21].

Characterization of the ceramics included diameter shrinkage, porosity and density, Vickers hardness, thermal expansion and dielectric constant. The porosity and density of the ceramics were determined using the Archimedes method following the Australian Standard No. 1774.5-2014. The Vickers hardness test was performed on the polished ceramic surface at 2 kgf for the B_2O_3-added samples and at 0.2 kgf for the B_2O_3-free sample. The linear thermal expansion coefficient of the ceramic samples was determined using a Mettler-Toledo© Thermomechanical Analyzer. A transmission phase-shift method was employed with an Advantest R3770 vector network analyzer connected to an A-INFOMW WG P/N 90WCAN rectangular waveguide to acquire the dielectric properties of the ceramics at a microwave frequency of 8–12 GHz. SEM micrographs were also collected on the surfaces of the sintered ceramics using an FEI Inspect-S50.

3. Results and discussion

3.1. Phase analysis

Table 1 presents the XRF data for the silica sand and its purified powder. The purification process increased the Si content by eliminating other "inorganic" elements, i.e., Cr, Ti, Fe, and K. The main residual element was Ti, which constituted as much as 0.5% of the purified silica powder. The XRD pattern of the powder (Fig. 1a) revealed that the powder contained only quartz (PDF# 46-1045). A highly crystalline quartz powder was observed based on the strong peaks of this phase.

Table 1
XRF "inorganic" elemental content of the silica sand and its purified powder.

Sample	Elemental content (at%)					
	Si	Cr	Ti	Fe	K	Others
Sand	94.7	0.9	1.6	0.8	0.5	1.5
Purified	98.7	0.3	0.5	0.3	0.1	0.1

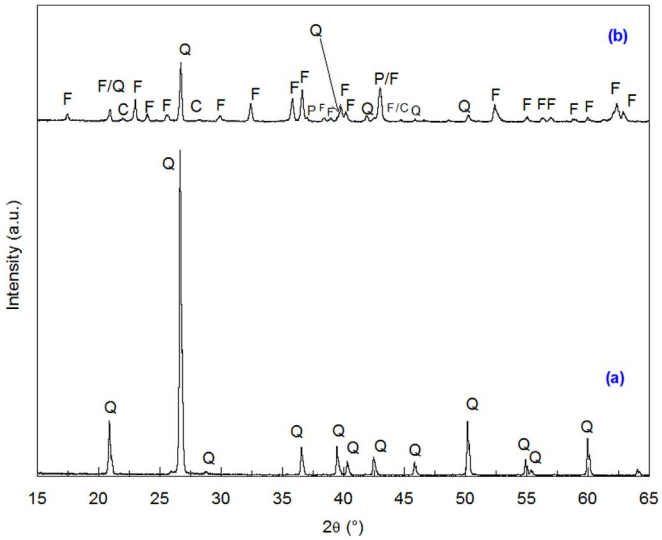

Fig. 1. XRD patterns (CuKα radiation) of the (a) silica powder after purification and (b) forsterite powder prior to the forsterite ceramic sintering. Label: Q – quartz (SiO_2), C – cristobalite (SiO_2), P – periclase (MgO), F – forsterite (Mg_2SiO_4).

This result proves that a relatively high purity quartz powder was achieved from the simple process of washing, magnetic separation, milling and 2 M HCl soaking of the silica sand.

The XRD pattern of the calcined silica-magnesia mixture at 1100 °C is presented in Fig. 1b. Calcination resulted in a powder containing forsterite (Mg_2AlSiO_4, PDF# 34-0189), quartz, cristobalite (SiO_2, PDF# 82-1232), and periclase (PDF# 45-0946). Forsterite is formed through the reaction

$$2MgO+SiO_2 \rightarrow Mg_2SiO_4 \quad (1)$$

In some cases, the solid reaction to form forsterite is completed above 1400 °C [19]. A Rietveld phase calculation using the 'ZMV' method embedded in the Rietica program [21] gave the relative weight fractions of the phases in the powder, which are listed in Table 2. *W* values for all phases were extracted after the fittings since the fitting figure-of-merits were acceptable, e.g., the goodness-of-fit was less than 4% and the fluctuation in the difference plots between the calculated

Table 2
Rietveld relative weight fraction of the phases in the calcined powder and sintered ceramics.

	Powder	Ceramic		
		0% B_2O_3	4% B_2O_3	8% B_2O_3
Forsterite (Mg_2SiO_4)	60.9 ± 1.3	88.1 ± 1.8	76.5 ± 1.5	53.4 ± 1.6
Quartz (SiO_2)	16.1 ± 0.5	5.5 ± 0.8	–	–
Cristobalite (SiO_2)	3.0 ± 0.3	6.4 ± 1.2	8.5 ± 1.0	21.2 ± 2.3
Periclase (MgO)	19.9 ± 0.7	–	–	–
Protoenstantite ($MgSiO_3$)	–	–	2.3 ± 0.2	4.0 ± 0.3
Clinoenstatite ($MgSiO_3$)	–	–	5.1 ± 0.3	8.9 ± 0.4
Suanit ($Mg_2B_2O_5$)	–	–	6.3 ± 0.4	12.1 ± 0.5
Rutile (TiO_2)	–	–	1.3 ± 0.2	0.4 ± 0.1

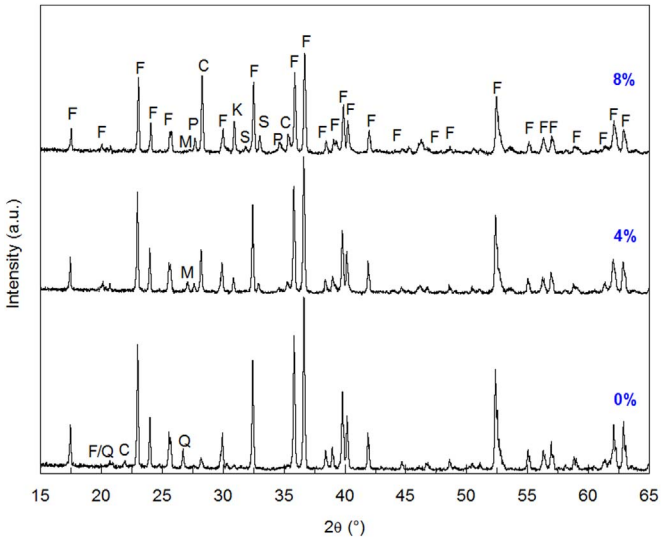

Fig. 2. XRD patterns (CuKα radiation) of the forsterite ceramics without and with addition of B_2O_3. Label: F – forsterite (Mg_2SiO_4), C – cristobalite (SiO_2), Q – quartz (SiO_2), P – protoenstatite ($MgSiO_3$), K – clinoenstatite ($MgSiO_3$), S – suanite ($Mg_2B_2O_5$), R – ruile (TiO_2).

and the observed patterns was insignificant [22]. The forsterite content (60.9 wt%) indicates that the reaction after calcination at 1100 °C was not complete. The raw materials (SiO_2 and MgO) were still present in the powder. The main quartz peak at 2θ≈26.5° dominated the pattern, but its Rietveld relative weight fraction was only 16.1%. However, in our case, a higher calcination temperature was not recommended because it could form large particles that would create difficulties in preparing the ceramics. Note that the forsterite powder contained no phases from minor inorganic elements.

Sintering the pressed B_2O_3-containing forsterite powders at 1200 °C produced ceramics whose XRD patterns are depicted in Fig. 2. In general, the phase compositions of the ceramics were different from and more complex than the original powder. Quartz became significantly less dominant and periclase (strongest peak at 2θ ≈43.1°) diminished. Forsterite became more dominant, indicating that the reaction in Eq. (1) was more complete. The reaction was driven by the greater thermal energy provided by increasing the sintering temperature. Meanwhile, the B_2O_3-added samples exhibited new phases, i.e., protoenstatite (PDF# 3-523), clinoenstatite ($MgSiO_3$, PDF# 35-610) and suanite ($Mg_2B_2O_5$, PDF# 15-537). Enstatite-group ($MgSiO_3$-group) phases are often observed during the synthesis of forsterite [12,14]. The formation of this 1:1 M ratio MgO-SiO_2 compound is attributed to the inhomogeneous mixing of the "flowing" constituent substances. Meanwhile, the presence of the liquid-phase suanite can be assigned to a stoichiometric reaction between MgO and B_2O_3. Suanite is responsible for the remarkable densification and hardness improvement of the ceramics, which will be discussed later.

In this work, TiO_2 (rutile) is present in the ceramic samples containing B_2O_3 but absent in the sample without B_2O_3. In our study, the addition of B_2O_3 appears to have caused the crystallization of TiO_2. The latter phase was not observed in the forsterite powder, but a relatively low level of Ti was observed in the raw materials by XRF spectroscopy (see Table 1).

The phase compositions of the ceramics are also reported in Table 2. The forsterite content decreased significantly from 88.1% in the B_2O_3-free ceramic to 53.4% in the 8%- B_2O_3 ceramic. Meanwhile, the presence of B_2O_3 induced two phenomena: (1) the presence of as much as 6% and 12% of suanite and (2) an increase in the amount of enstatite from only 6% to approximately 25%. These phenomena can explained as follows: upon sintering, B_2O_3 melts at approximately 480 °C [23]. It then "flows" through the pores of the compacted pellets

Table 3
Rietveld-derived lattice parameters and unit cell volume of forsterite in the sintered forsterite ceramics.

Parameters	0%	4%	8%
a (Å)	4.6834 ± 0.0003	4.6804 ± 0.0003	4.6803 ± 0.0005
b (Å)	10.0584 ± 0.0005	10.0626 ± 0.0005	10.0650 ± 0.0010
c (Å)	5.8975 ± 0.0003	5.9000 ± 0.0003	5.9007 ± 0.0006
Volume ($Å^3$)	277.82 ± 0.03	277.86 ± 0.03	277.98 ± 0.05

before reacting with MgO to form $Mg_2B_2O_5$ at approximately 750 °C [24]. The subsequent reaction depends on the MgO-SiO_2 composition, i.e., either forming enstatite-group phases (1:1 MgO-SiO_2 composition ratio) or forsterite (2:1 ratio). Therefore, the presence of more B_2O_3 causes the formation of more suanite, thereby reducing the amount of MgO that can pair with SiO_2 to produce more cristobalite and enstatite, and decreases the amount of forsterite that is formed. The amount of rutile in the B_2O_3-added ceramics was less than 1.5 wt%, but the phase was absent in the B_2O_3-free ceramic. Again, the presence of B_2O_3 appears to have induced the formation of rutile in the ceramics. Interestingly, the presence of a low level of TiO_2 in the forsterite ceramic system may reduce the sintering temperature by 100 °C [25]. It is therefore argued that TiO_2 favored the densification of our B_2O_3-added ceramics.

The effect of B_2O_3 addition on the structure of forsterite was determined from the Rietveld-derived cell parameters (Table 3). Forsterite exhibits an orthorhombic structure with a space group of *Pbnm* [26]. During sintering of the B_2O_3-added ceramics, the glassy phase appears to have favored the expansion of the forsterite crystal in the *b* and *c* directions and suppressed expansion in the *a* direction. For example, compared to the B_2O_3-free ceramic, the *a* value in the 4% B_2O_3-added ceramic decreased by −0.3% and the *b* and *c* values increased by 0.4% and 0.3%, respectively. As a consequence of these changes, the overall cell volume increased with the addition of B_2O_3. The difference in the changes of these parameters can be ascribed to the difference in the crystallographic elastic moduli. The elastic modulus of forsterite in the *a* direction is larger than that in the *b* and *c* directions [27], with crystallographic modulus value ratios $E(b/a)$ and $E(c/a)$ of approximately 0.61 and 0.72, respectively. The presence of the "flowing" phase eased the expansion of the low elastic modulus axes (in this case the *b* and *c* axes) and consequently stretched the stronger one (*a* axis). Therefore, the addition of B_2O_3 changed the structure of forsterite in the ceramics.

3.2. Characteristics of the ceramics

In this work, we also observed that the presence of B_2O_3 obviously affected the physical properties of the forsterite ceramics (Table 4). While the B_2O_3-free ceramic shrank by only 0.3%, the diameter of the B_2O_3-added ceramics decreased by more than 21%. Moreover, the porosity and density of these two ceramics were also very different, with densities of 1.27 and 3.09 g cm^{-3} and porosities of nearly 40% and 0.3%, respectively. The densities of forsterite, quartz, cristobalite, protoenstatite, clinoenstatite, suanite, and rutile are 3.06, 2.65, 2.32, 3.20, 3.11, 2.91 and 4.27, respectively [28]. The presence of the

Table 4
Shrinkage (*S*), apparent density (*D*), apparent porosity (*P*), Vickers hardness (H_v) and linear thermal expansion coefficient (*α*) of the forsterite ceramics.

B_2O_3	*S* (%)	*D* (g cm^{-3})	*P* (%)	H_v (GPa)	*α* (ppm/°C)
0%	0.3	1.27	39.6	0.3	18.4
4%	24.3	3.01	0.3	10.9	12.1
8%	21.3	3.09	0.7	8.5	10.4

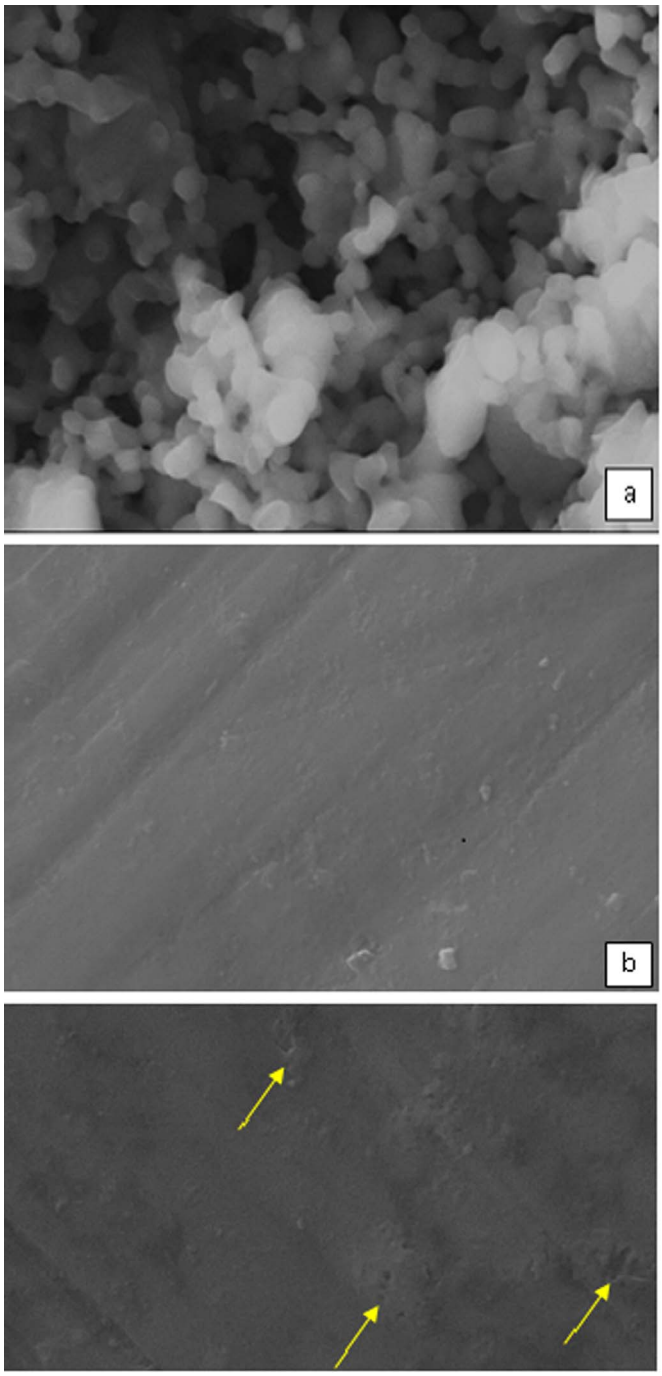

Fig. 3. SEM micrographs of the surface of the forsterite ceramic samples without B_2O_3 (a), with 4% (b) and 8% (c) B_2O_3.

"glassy" suanite phase is believed to favor the densification of ceramics. This densification behavior was confirmed by SEM micrographs of the polished surfaces of the ceramics that are depicted in Fig. 3. The surfaces of the 4% and 8% samples were significantly denser than the B_2O_3-free sample. The 8% sample exhibited "buldging" on the surface (arrows), which explains the slight increase in its porosity (Table 4).

The Vickers hardness value increased drastically from 0.3GPa to 10.9 GPa (Table 4). The significant increase in the Vickers hardness is due to the densification of the ceramic as a result of the introduction of B_2O_3. The hardness of a material containing a glassy or liquid phase depends on the number of topological constraints between atoms or crystalline phases in the network. The planes of atoms in the crystalline phases experience slips that produce dislocations and thus permanent deformation. These planes can easily propagate from one part of the material to another in soft materials. When a liquid phase such as $Mg_2B_2O_5$ is located between crystalline grains, it will withstand the propagation of the planes and permanent deformation, thereby creating a harder material. In our work, the deformation of the porous B_2O_3-free sample was massive compared to the very dense B_2O_3-containing samples. The liquid phase $Mg_2B_2O_5$ appears to fill the porosity and resist the propagation of deformation planes.

The linear thermal expansion coefficients (α) of the forsterite ceramics between room temperature and 1000 °C are presented in Table 4. We found an anomalous linear thermal expansion behavior of the ceramics in terms of porosity. Typically, α decreases with increasing porosity, but we observed the opposite trend in our samples. This property is certainly influenced by the phase composition. Among the phases present in the samples, quartz exhibited the highest α, i.e., 24.3, followed by protoenstatite with a value of 16.7, while the others were in the range 8–10. The combination of porosity and phase composition affects the linear thermal expansion of the ceramic composites. However, further investigation on the contribution of each component is required to better understand the phenomenon.

Fig. 3 presents the dielectric properties of the ceramics. The B_2O_3-free ceramic exhibited relatively frequency-independent dielectric properties with an ε' value of approximately 5. This can be attributed to the fact that the dielectric constants of forsterite, quartz, cristobalite, proto- and clino-enstatite, and suanite are relatively low, i.e., in the range 4–7, while TiO_2 (rutile) is approximately 100 [19,29–34]. Morever, the ceramic exhibited high porosity, which may lower ε' [35].

Fig. 3 also shows that ε' of the B_2O_3-added forsterite ceramics is 2–6 times greater than that of the B_2O_3-free ceramic depending on the frequency. The dielectric constant rise in our complex ceramics can be attributed to three phenomena. First, the presence of a liquid $Mg_2B_2O_5$ phase may change the dielectric constant value through the volatilization of B_2O_3. This causes a higher polarization of Mg^{2+} than B^{3+} [29] and hence a higher dielectric constant. However, the contribution of such polarization is relatively small. Second, the presence of high dielectric constant TiO_2 (rutile) has an effect on the dielectric properties of the B_2O_3-added ceramics. However, the rutile content is low, i.e., only approximately 1.2 and 0.4 wt% (Table 2). Although rutile exhibits a higher dielectric constant than the other phases, its contribution is also relatively low. Calculating the contribution of rutile using the rule of mixture, we found that with 0.9 and 0.3 vol% rutile in the ceramics, the increase in ε' does not exceed 3%. A similar minor improvement of ε' in forsterite ceramics by TiO_2 was reported [11]. The third origin is the drastic reduction in porosity, which can be tremendous [35,36]. In alumina ceramics [35], when the porosity decreased from 40% to 1%, the microwave dielectric constant doubled. A similar multiplied dielectric constant phenomenon was also observed in $Mg_3(VO_4)_2$ ceramics [36]. There was also a report on the effect of density, which is inversely proportional to porosity, on the dielectric constant of silicon nitride ceramics [37], i.e., ε' was 8 for a density of 3.2 g cm^{-3} and 5.7 for a density of 2.4 g cm^{-3}. A denser ceramic exhibits a higher grain boundary density and hence a higher dielectric constant [38,39]. It is then argued that the main cause of the vast increase in ε' in the B_2O_3-added forsterite ceramics was the excellent densification of the ceramics. Therefore, our forsterite porous and dense ceramics exhibited low and medium-permitivity at the frequency range between 8 and 12 GHz which is appropriate for millimeter-wave communication systems and base station for wireless Local Area Network and Intelligent Transport System respectively [30]. In addition, we observed here that the ceramics exhibited a strong dependence of the ε' value on frequency (Fig. 4).

4. Conclusion

Extremely dense forsterite-based ceramics were successfully fabricated using purified natural silica sand as the silica source and

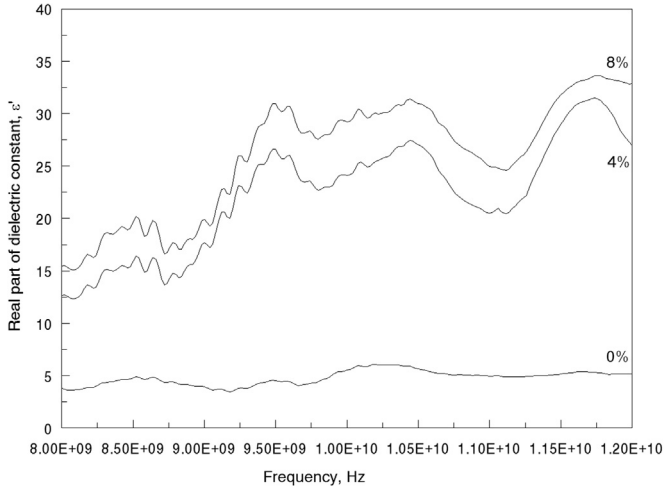

Fig. 4. Dielectric constant (real part) of the forsterite ceramic samples without B_2O_3, with 4% and 8% B_2O_3.

magnesium oxide powder with the addition of 4 and 8 wt% B_2O_3 as a sintering agent. Sintering at 1200 °C resulted in relatively complex ceramic composites consisting of forsterite, quartz, cristobalite, enstatite, suanite and rutile. The densification process was thoroughly explained in terms of phase composition and structure. The B_2O_3-added forsterite ceramics exhibited only 1% porosity, which is responsible for the improvement in the Vickers hardness as well as the dielectric constant value. Investigation on the dielectric properties showed that the B_2O_3-added forsterite ceramics possess a medium-permitivity character which is appropriate for permanent and mobile communication instruments. The ceramics exhibited anomalous linear thermal expansion behavior, which requires further investigation.

Acknowledgement

The authors would like to express gratitude to the Ministry of Research Technology and Higher Education of the Republic of Indonesia and Institute for Research and Community Services ITS for the support of research funding through the PUPT program Contract No. 01751/IT2.11/PN.08/2016.

References

[1] A. Teimouri, L. Ghorbanian, A.N. Chermahini, R. Emadi, Fabrication and characterization of silk/forsterite composites for tissue engineering applications, Ceram. Int. 40 (2014) 6405–6411.
[2] H. Ohsato, T. Tsunooka, T. Sugiyama, K. Kakimoto, H. Ogawa, Forsterite ceramics for millimeterwave dielectrics, J. Electroceram. 17 (2006) 445–450.
[3] C.Y. Tan, R. Singh, Y.C. Teh, Y.M. Tan, B.K. Yap, Sinterability of forsterite prepared via solid-state reaction, Int. J. Appl. Ceram. Technol. 12 (2013) 437–442.
[4] T. Tsunooka, M. Ando, S. Suzuki, Y. Yasufuku, H. Ohsato, Research & developments for millimeter-wave dielectric forsterite with low dielectric constant, high *Q*, and zero temperature coefficient of resonant frequency, Jpn. J. Appl. Phys. 52 (2013) 09KH02.
[5] S. Ni, L. Chou, J. Chang, Preparation and characterization of forsterite (Mg_2SiO_4) bioceramics, Ceram. Int. 33 (2007) 83–88.
[6] M.A. Naghiu, M. Gorea, E. Mutch, F. Kristaly, M. Tomoaia-Cotisel, Forsterite nanopowder: structural characterization and biocompatibility evaluation, J. Mater. Sci. Technol. 29 (2013) 628–632.
[7] C. Kosanović, N. Stubičar, N. Tomašić, V. Bermanec, M. Stubičar, Synthesis of a forsterite powder by combined ball milling and thermal treatment, J. Alloy. Compd. 389 (2005) 306–309.
[8] F.S. Sayyedan, M.H. Fathi, H. Edris, A. Doostmohammadi, V. Mortazavi, A. Hanifi, Effect of forsterite nanoparticles on mechanical properties of glass ionomer cements, Ceram. Int. 40 (2014) 10743–10748.
[9] M.H. Fathi, M. Kharaziha, Two-step sintering of dense, nanostructural forsterite, Mater. Lett. 63 (2009) 1455–1458.
[10] H. Barzegar Bafrooei, T. Ebadzadeh, H. Majidian, Microwave synthesis and sintering of forsterite nanopowder produced by high energy ball milling, Ceram. Int. 40 (2014) 2869–2876.
[11] E. Bernardo, L. Fiocco, G.A. Giffin, V. Di Noto, P. Colombo, Microstructure development and dielectric characterization of forsterite-based ceramics from silicone resins and oxide fillers, Adv. Eng. Mater. 16 (2014) 806–813.
[12] M.H. Fathi, M. Kharaziha, Mechanically activated crystallization of phase pure nanocrystalline forsterite powders, Mater. Lett. 62 (2008) 4306–4309.
[13] M. Kharaziha, M.H. Fathi, Synthesis and characterization of bioactive forsterite nanopowder, Ceram. Int. 35 (2009) 2449–2454.
[14] S. Ramesh, A. Yaghoubi, K.Y. Sara Lee, K.M. Christopher Chin, J. Purbolaksono, M. Hamdi, M.A. Hassan, Nanocrystalline forsterite for biomedical applications: synthesis, microstructure and mechanical properties, J. Mech. Behav. Biomed. Mater. 25 (2013) 63–69.
[15] M.I. Martín, F. Andreola, L. Barbieri, F. Bondioli, I. Lancellotti, J.M. Rincón, M. Romero, Crystallisation and microstructure of nepheline–forsterite glass-ceramics, Ceram. Int. 39 (2013) 2955–2966.
[16] L. Chen, G. Ye, Q. Wang, B. Blanpain, A. Malfliet, M. Guo, Low temperature synthesis of forsterite from hydromagnesite and fumed silica mixture, Ceram. Int. 41 (2015) 2234–2239.
[17] U. Nurbaiti, Triwikantoro, M. Zainuri, S. Pratapa, Synthesis of microforsterite using derived-amorphous-silica of silica sands, in: AIP Conference Proceedings, AIP Publishing, 2016, p. 020056.
[18] E.M. El-Meliegy, E.M.A. Hamzawy, Celsian–fluorophlogopite porcelain based on Egyptian talc, Adv. Appl. Ceram. 104 (2005) 92–96.
[19] S. Sano, N. Saito, S.-I. Matsuda, N. Ohashi, H. Haneda, Y. Arita, M. Takemoto, Synthesis of high density and transparent forsterite ceramics using nano-sized precursors and their dielectric properties, J. Am. Ceram. Soc. 89 (2006) 568–574.
[20] C.-Y. Liu, B.-G. Tsai, M.-H. Weng, S.-J. Huang, Influence of B_2O_3 additive on microwave dielectric properties of $Li_2ZnTi_3O_8$ ceramics for LTCC applications, Int. J. Appl. Ceram. Technol. 10 (2013) E49–E56.
[21] B.A. Hunter, Rietica, newsletter of international union of crystallography, Comm. Powder Diffr. 20 (1998) 21.
[22] R.A. Young, Introduction to the Rietveld method, Rietveld Method. 5 (1993) 1–38.
[23] S.-F. Wang, Y.-R. Wang, Y.-F. Hsu, C.-C. Chuang, Effect of additives on the thermal properties and sealing characteristic of BaO-Al_2O_3-B_2O_3-SiO_2 glass-ceramic for solid oxide fuel cell application, Int. J. Hydrogen Energy 34 (2009) 8235–8244.
[24] A. Üçyıldız, İ. Girgin, Controlled synthesis, characterization and thermal properties of $Mg_2B_2O_5$, Open Chem. 8 (2010).
[25] T. Tsunooka, M. Androu, Y. Higashida, H. Sugiura, H. Ohsato, Effects of TiO_2 on sinterability and dielectric properties of high-*Q* forsterite ceramics, J. Eur. Ceram. Soc. 23 (2003) 2573–2578.
[26] R.M. Hazen, Effects of temperature and pressure on the crystal structure of forsterite, Am. Mineral. 61 (1976) 1280–1293.
[27] D.G. Isaak, O.L. Anderson, T. Goto, I. Suzuki, Elasticity of single-crystal forsterite measured to 1700 K, J. Geophys. Res.: Solid Earth 94 (1989) 5895–5906.
[28] T.J. Ahrens, Mineral Physics & Crystallography: A Handbook of Physical Constants, American Geophysical Union, Washington, DC, 1995.
[29] G. Fan, H. Zhou, X. Chen, Optimized sintering temperature and enhanced microwave dielectric performance of $Mg_2B_2O_5$ ceramic, J. Mater. Sci: Mater. Electron. (2016) 1–5.
[30] H. Ohsato, T. Tsunooka, M. Ando, Y. Ohishi, Y. Miyauchi, K. Kakimoto, Millimeter-wave dielectric ceramics of alumina and forsterite with high quality factor and low dielectric constant, J. Korean Ceram. Soc. 40 (2003) 350–353.
[31] M.-E. Song, J.-S. Kim, M.-R. Joung, S. Nahm, Y.-S. Kim, J.-H. Paik, B.-H. Choi, Synthesis and microwave dielectric properties of $MgSiO_3$ ceramics, J. Am. Ceram. Soc. 91 (2008) 2747–2750.
[32] G.N. Sun, E.S. Kim, Microwave dielectric properties of diopside-enstatite glass-ceramics, Ferroelectrics 434 (2012) 44–51.
[33] W. Volksen, R.D. Miller, G. Dubois, Low dielectric constant materials, Chem. Rev. 110 (2010) 56–110.
[34] C. Wang, N. Zhang, Q. Li, Y. Yu, J. Zhang, Y. Li, H. Wang, Dielectric relaxations in rutile TiO_2, J. Am. Ceram. Soc. 98 (2015) 148–153.
[35] S.J. Penn, N.M. Alford, A. Templeton, X. Wang, M. Xu, M. Reece, K. Schrapel, Effect of porosity and grain size on the microwave dielectric properties of sintered alumina, J. Am. Ceram. Soc. 80 (1997) 1885–1888.
[36] R. Umemura, H. Ogawa, H. Ohsato, A. Kan, A. Yokoi, Microwave dielectric properties of low-temperature sintered $Mg_3(VO_4)_2$ ceramic, J. Eur. Ceram. Soc. 25 (2005) 2865–2870.
[37] V.R.K. Murthy, S. Sundaram, B. Viswanathan, Microwave Materials, Springer, 1994.
[38] P. Lunkenheimer, V. Bobnar, A.V. Pronin, A.I. Ritus, A.A. Volkov, A. Loidl, Origin of apparent colossal dielectric constants, Phys. Rev. B. 66 (2002).
[39] G. Zang, J. Zhang, P. Zheng, J. Wang, C. Wang, Grain boundary effect on the dielectric properties of $CaCu_3Ti_4O_{12}$ ceramics, J. Phys. D: Appl. Phys. 38 (2005) 1824–1827.